AGU PUBLICATIONS

JGR

Journal of Geophysical Research: Atmospheres

RESEARCH ARTICLE
10.1002/2013JD021169

Key Points:
- Nitrates in atmospheric particles may react with water-soluble organic acids
- Aging of mixed organic/nitrate particles modifies their composition
- Nitrate/organics reactivity is determined for atmospherically relevant particles

Supporting Information:
- Readme
- Figure S1
- Figure S2
- Figure S3

Correspondence to:
A. Laskin,
Alexander.Laskin@pnnl.gov

Citation:
Wang, B., and A. Laskin (2014), Reactions between water-soluble organic acids and nitrates in atmospheric aerosols: Recycling of nitric acid and formation of organic salts, *J. Geophys. Res. Atmos.*, *119*, doi:10.1002/2013JD021169.

Received 7 NOV 2013
Accepted 19 FEB 2014
Accepted article online 23 FEB 2014

Reactions between water-soluble organic acids and nitrates in atmospheric aerosols: Recycling of nitric acid and formation of organic salts

Bingbing Wang[1] and Alexander Laskin[1]

[1]William R. Wiley Environmental Molecular Sciences Laboratory, Pacific Northwest National Laboratory, Richland, Washington, USA

Abstract Atmospheric particles often include a complex mixture of nitrate and secondary organic materials accumulated within the same individual particles. Nitrate as an important inorganic component can be chemically formed in the atmosphere. For instance, formation of sodium nitrate ($NaNO_3$) and calcium nitrate ($Ca(NO_3)_2$) occurs when nitrogen oxides and nitric acid (HNO_3) react with sea salt and calcite, respectively. Organic acids contribute a significant fraction of photochemically formed secondary organics that can condense on the preexisting nitrate-containing particles. Here we present a systematic microanalysis study on chemical composition of laboratory-generated particles composed of water-soluble organic acids and nitrates (i.e., $NaNO_3$ and $Ca(NO_3)_2$) using computer-controlled scanning electron microscopy with energy-dispersive X-ray microanalysis and Fourier transform infrared microspectroscopy. The results show that water-soluble organic acids can react with nitrates and release gaseous HNO_3 during the dehydration process. These reactions are attributed to acid displacement of nitrate with weak organic acids driven by the evaporation of HNO_3 into gas phase because of its relatively high volatility. The reactions result in significant nitrate depletion and formation of organic salts in mixed organic acids/nitrate particles that, in turn, may affect their physical and chemical properties relevant to atmospheric environment and climate. Airborne nitrate concentrations are estimated by thermodynamic calculations corresponding to various nitrate depletions in selected organic acids of atmospheric relevance. The results indicate a potential mechanism of HNO_3 recycling that may further affect concentrations of gas and condensed phase species in the atmosphere and the heterogeneous reaction chemistry between them.

1. Introduction

Ambient aerosol particles play important roles in atmospheric chemistry, air quality, global radiation budget, hydrological cycle, and public health [e.g., *Fiore et al.*, 2012; *Forster et al.*, 2007; *Heal et al.*, 2012; *Pöschl*, 2005; *Ramanathan et al.*, 2001]. Aerosol particles can affect the radiation directly by scattering and absorbing solar and terrestrial radiation, and indirectly through aerosol-cloud interactions by acting as cloud condensation and ice nuclei [e.g., *Albrecht*, 1989; *Baker*, 1997; *Knopf et al.*, 2010; *Lohmann and Feichter*, 2005; *Ramanathan et al.*, 2001; *Rosenfeld*, 2000; *Wang et al.*, 2012a, 2012b]. Particles also serve as heterogeneous reaction sites for multiphase chemistry that alter condensed and gas phase compositions and thus affect atmospheric composition and air quality [*Abbatt et al.*, 2012; *Andreae and Crutzen*, 1997; *Ravishankara*, 1997; *Rudich*, 2003]. All these effects depend on the chemical and physical properties of particles, such as composition, sizes, optical refractivity, hygroscopicity, and chemical reactivity.

Internal composition of individual ambient particles is typically a complex mixture of organic and inorganic materials from various biogenic and anthropogenic sources. Atmospheric organic materials can contain thousands of individual species and contribute, overall, a significant mass fraction of primary and secondary fine particulate matter [*Jimenez et al.*, 2009; *Kanakidou et al.*, 2005; *Murphy et al.*, 2006; *Zhang et al.*, 2007]. Atmospheric aging of primary and secondary organics increases the oxidation state of carbon and forms more oxygenated organic species such as carboxylic acids [e.g., *Jimenez et al.*, 2009; *Kroll et al.*, 2011; *Rudich*, 2003]. Water-soluble organic acids, including dicarboxylic acids, such as malonic and glutaric acid, are a group of organic compounds often detected in atmospheric particles [*Chebbi and Carlier*, 1996; *Kawamura and Kaplan*, 1987; *Saxena and Hildemann*, 1996; *Yang and Yu*, 2008].

Various inorganic materials, including sulfate, nitrate, sea salt, and dust are ubiquitous components in ambient particles that are often internally mixed with organics in different environments. Most of the nitrates are formed from atmospheric reactions of nitrogen species, including N_2O_5, NO_3, and HNO_3 with NH_3 and

aerosol particles, including sea salt and mineral dust [*Seinfeld and Pandis*, 1998]. Most common and most abundant forms of nitrate in ambient particles are NH_4NO_3, $NaNO_3$, and $Ca(NO_3)_2$ [*Seinfeld and Pandis*, 1998]. Nitrate aerosols may become even more abundant in the atmosphere in the future because of the expected increase in the emission of their precursors [e.g., *Bauer et al*., 2007]. Atmospheric HNO_3 is the oxidation product of NO_x and is a reservoir of reactive odd nitrogen (NO_y) that plays an important role in atmospheric nitrogen chemistry and nitrate formation [*Brown and Stutz*, 2012; *Seinfeld and Pandis*, 1998].

Mineral dust and sea salt are ubiquitous inorganic particles emitted from natural sources of desert areas and oceans, respectively [*Lewis and Schwartz*, 2004; *Mahowald et al*., 2005; *Murphy et al*., 2006; *Usher et al*., 2003; *Zhang et al*., 2007]. In the atmosphere, these particles undergo atmospheric aging that may substantially modify their composition resulting in changes to chemical and physical properties [*Abbatt et al*., 2012; *Finlayson-Pitts*, 2003; *Rossi*, 2003; *Rudich*, 2003; *Usher et al*., 2003]. Sea salt and mineral dust particles react with different oxides and inorganic acids, such as NO_3 and HNO_3 [e.g., *Ault et al*., 2013; *Baltrusaitis and Grassian*, 2012; *Finlayson-Pitts*, 2003; *Gard et al*., 1998; *Rossi*, 2003; *Song et al*., 2013; *Usher et al*., 2003]. Field and laboratory studies have shown that heterogeneous reactions of sea salt and mineral dust with nitrogen oxides and HNO_3 convert NaCl into $NaNO_3$, whereas $CaCO_3$ is converted to $Ca(NO_3)_2$ [e.g., *Finlayson-Pitts*, 2003; *Gibson et al*., 2006; *Krueger et al*., 2003; *Laskin et al*., 2005a, 2005b; *Liu et al*., 2007, 2008; *Rubasinghege and Grassian*, 2013]. Other mineral dust components and metal oxides, including $CaMg(CO_3)_2$, CaO, $Ca(OH)_2$, MgO, Al_2O_3, TiO_2, Fe_2O_3, and FeOOH, could also react with HNO_3 and nitrogen oxides and contribute to nitrate formation [*Chen et al*., 2011; *Johnson et al*., 2005; *Laskin et al*., 2005b; *Rubasinghege and Grassian*, 2013; *Vlasenko et al*., 2009; *Wijenayaka et al*., 2012].

There is a growing amount of literature showing that organic acids are important contributors to the particle aging chemistry of mineral dust and sea salt that can proceed through both gas-particle reactions [*Ma et al*., 2012; *Tong et al*., 2010; *Usher et al*., 2003] and aqueous reactions between organic acids and inorganics within individual particles [*Kerminen et al*., 1998; *Laskin et al*., 2012; *Laskina et al*., 2013; *Ma et al*., 2013]. Recently, we showed that water-soluble organic acids can effectively react with sea salt particles resulting in chloride depletion [*Laskin et al*., 2012]. Gaseous HCl can be released from aerosolized sea salt particles as a result of acid displacement between NaCl and secondary organic materials through a reaction mechanism (R1) driven by the high volatility of gas phase HCl product [*Laskin et al*., 2012].

$$NaCl_{(aq)} + HA\,(org)_{(aq,g)} \leftrightarrow NaA\,(org)_{(aq,s)} + HCl_{(aq,g)}\uparrow \quad \text{(R1)}$$

Here HA(org) represents a range of carboxylic acids present as condensed phase organic matter in atmospheric particles. We attributed this reaction to our observations of the chloride depletion in internally mixed sea salt/organic particles collected on board research aircraft during a field study in the vicinity of Sacramento, CA [*Laskin et al*., 2012]. Those observations were also corroborated in a set of laboratory experiments where mixed particles composed of NaCl, and selected organic acids showed similar effects of chloride depletion, although different organic acids exhibited different potentials to deplete chloride [*Laskin et al*., 2012]. The possible extent of these reactions at different ambient conditions and aerosol concentrations was then evaluated based on the calculations of gas/particle partitioning of HCl in selected aerosol systems using the Extended Aerosol Inorganics Model (E-AIM, http://www.aim.env.uea.ac.uk/aim/aim.php) [*Clegg and Seinfeld*, 2006a, 2006b; *Laskin et al*., 2012]. The result showed that thermodynamically favored gas phase release of HCl shifts equilibrium of reaction (R1) to the right and controls the chemical composition of resulted particles. Notably, substantial levels of chloride depletion (20–50%) were estimated for mixed NaCl/malonic acid particles aerosolized at atmospherically relevant concentrations (10–100 $\mu g\,m^{-3}$) and relative humidity (RH) (30–50%) [*Laskin et al*., 2012; *Lewis and Schwartz*, 2004].

In this work, we present experimental results and corresponding E-AIM modeling calculations on internally mixed HA(org)/nitrate particles. We show that similar acid displacement reactions can be also driven by gas phase release of HNO_3 and its partitioning between condensed and gas phases resulting in nitrate depletion and formation of organic salts as the following:

$$NaNO_{3\,(aq)} + HA\,(org)_{(aq,g)} \leftrightarrow NaA\,(org)_{(aq,s)} + HNO_{3\,(aq,g)}\uparrow \quad \text{(R2)}$$

To better understand these interactions between HA(org) and nitrate particles, we conducted systematic studies on the reactions of selected HA(org) particles, including malonic acid (MA), malic acid (Malic), tartaric

Table 1. Summary of Mean N/Na and N/Ca* Ratios With 1 Standard Deviation for the Investigated Particle Samples of Mixed HA(org)/Nitrate[a]

		N/Na and N/Ca* Ratios Measured in Particles[b]			
		$NaNO_3$		$Ca(NO_3)_2$	
Organic Acids, HA(org)	Mixing Ratio in Solution	Fresh Particles[c]	Stored Particles[c]	Fresh Particles[c]	Stored Particles[c]
Malonic acid (MA)	1:3	0.65 ± 0.20	-	0.64 ± 0.22	-
	1:1	0.45 ± 0.20	0.20 ± 0.12	0.38 ± 0.16	0.18 ± 0.12
	3:1	0.10 ± 0.10	-	(0.2–0.6) ± 0.2	-
Glutaric acid (GA)	1:1	0.63 ± 0.15	0.50 ± 0.20	(0.6–1.0) ± 0.2	(0.2–0.6) ± 0.2
Malic acid (Malic)	1:1	0.55 ± 0.15	0.36 ± 0.17	0.49 ± 0.16	0.29 ± 0.21
Tartaric acid (TA)	1:1	0.41 ± 0.12	0.10 ± 0.08	-	-
Citric acid (CA)	1:1	0.51 ± 0.17	0.20 ± 0.18	(0.2–0.6) ± 0.2	(0.1–0.3) ± 0.1

[a]Molar ratios of HA(org) to nitrate are also listed for solutions used for particle generation.
[b]N/Ca* ratios listed here are experimentally measured values normalized to the reference ratios of $Ca(NO_3)_2$ particle standards. (See Figure 4 and associated discussion for details.)
[c]The samples analyzed within 24 h after generation were termed as "fresh sample". The samples that were stored for 4 weeks at 295 K and <45% RH were termed as "stored sample".

acid (TA), glutaric acid (GA), and citric acid (CA) with $NaNO_3$ and $Ca(NO_3)_2$. Microspectroscopy particle analysis was conducted using complementary techniques of computer-controlled scanning electron microscopy with energy-dispersive X-ray microanalysis (CCSEM/EDX) and Fourier transform infrared microspectroscopy (micro-FTIR). Elemental composition of individual particles determined by CCSEM/EDX was used to assess the reactivity of different HA(org) and their nitrate depletion potentials. Formation of organic salts and their characteristic chemical functionality were confirmed by mid-infrared vibrational spectra acquired using a micro-FTIR setup. Potential atmospheric implications of the reactions between organic acids and nitrates are also discussed.

2. Experimental Section

2.1. Sample Preparation

Particles were generated from aqueous solutions of mixed HA(org) and $NaNO_3$ (or $Ca(NO_3)_2$) at different molar ratios with total concentration of 0.5 *M*. $NaNO_3$ (99.5%), $Ca(NO_3)_2$ (99%), monosodium citrate ($C_6H_7O_7Na$, 99.5%), malonic acid (99%), DL-malic acid (99%), DL-tartaric acid (99.5%), glutaric acid (99%), and citric acid (99.5%) were obtained from Sigma-Aldrich, Co. LLC, and used without further purification. Deionized water (resistivity ≥ 18 *M*Ω cm) was used to prepare the solutions. Aqueous particles were first nebulized from solutions and then were dehydrated by passing through a diffusion dryer. The RH at the end of the dryer was measured and was <35% (Sensirion Inc., model SHT75). The airborne particles were collected onto grid-supported thin carbon film substrates used for transmission electron microscopy (Copper 400 mesh grids coated with Carbon Type-B films, Ted Pella, Inc.) and silicon nitride membrane windows (Si_3N_4 windows, Silson Ltd.) placed on the fourth, fifth, and sixth stages (cutoff sizes, D_{50} = 3.3, 1.8, and 1.0 μm) of a multiorifice uniform deposition impactor (model 110-R, MSP, Inc.). Particle samples were prepared in the same manner for all investigated particle compositions. Particles collected on the carbon-filmed grids and Si_3N_4 windows were used for CCSEM/EDX and micro-FTIR analysis, respectively. At least three independent samples were analyzed for each particle composition. Fresh particle samples were analyzed within 24 h after generation. Additional sets of selected samples were stored at room temperature (295 ± 1 K) and 25%–45% RH after generation for ~4 weeks and then were reanalyzed. These stored samples served to estimate maximum nitrate depletion by HA(org) at these conditions (295 K and <45% RH). Table 1 summarizes the investigated HA(org)/nitrate samples and the molar ratio of HA(org) to nitrate in solution used for particle generation. We note that particle samples generated from solution at a specific molar ratio of HA(org) to nitrate are referred as "HA(org)/nitrate (molar ratio)" throughout the manuscript. For instance, particles generated from MA/$NaNO_3$ solution at 1:1 molar ratio will be referred as "MA/$NaNO_3$ (1:1) particles".

2.2. CCSEM/EDX and Micro-FTIR Analysis

CCSEM/EDX analysis was used to determine the size, morphology, and quantitative elemental composition of individual particles, whereas micro-FTIR analysis was used to identify and quantify functional groups in investigated particle samples.

The environmental scanning electron microscope (SEM) (Quanta 3-D model, FEI, Inc.) used in this study is coupled with an EDAX X-ray spectrometer (EDAX Inc.) and a Si(Li) detector with an active area of 10 mm^2 and an Atmospheric Thin Window (ATW2) window [*Laskin et al*., 2012; *Wang et al*., 2012b]. During CCSEM/EDX analysis, particles deposited on the carbon-filmed grids were first identified and imaged using detection of either transmitted electron (TE) signal or secondary electron (SE) signal. Then, X-ray spectra for each of the identified particles were acquired at a beam current of 110 pA and an acceleration voltage of 20 kV for 5 s. Elemental compositions and equivalent circle diameters of individual particles were determined from recorded X-ray spectra and SEM images, respectively. Particle elemental composition is reported in terms of atomic fractions and their ratios. Because of low X-ray energy characteristic peak and possible beam damage, particles with an equivalent circle diameter larger than 0.9 μm were analyzed to minimize experimental artifacts. More details for the individual particle analysis by CCSEM/EDX on thin carbon-filmed grids can be found elsewhere [*Laskin*, 2010; *Laskin and Cowin*, 2001; *Laskin et al*., 2006, and references therein].

A detailed description of the micro-FTIR experimental setup has been reported elsewhere [*Cain et al*., 2010; *Liu et al*., 2008]. Briefly, the micro-FTIR apparatus consists of a Bruker A590 IR optical microscope coupled with a Bruker IFS66/S FTIR spectrometer and a mercury-cadmium-telluride detector. A sealable environmental sample stage (Linkam, FTIR 600), which allows IR beam passage through an optically transparent sample, is attached to the optical microscope. A Si_3N_4 window loaded with particles was placed onto and sealed in the sample stage. By moving the sample within the stage, the IR beam was positioned to pass through the particle sample. Dry nitrogen was used as purging gas to reduce the amount of CO_2 and water vapor present along the pathway of the IR beam. Samples were purged by dry nitrogen at 1 L/min for 30 min before spectra were collected. Background spectra were acquired using a separated particle-free Si_3N_4 "reference" window. All spectra were collected in transmission mode by coadding 512 individual scans between 4000 cm^{-1} and 500 cm^{-1} at a spectral resolution of 4 cm^{-1}. Averages of five background spectra were used as reference spectra for particle samples. For each sample, average of 15 spectra was used for further data analysis. All spectra were acquired with 0.3 mm aperture at 295 ± 0.5 K and dry conditions (RH < 10%). All the sample spectra were acquired over an ensemble of a few hundred particles.

3. Results and Discussions

3.1. Particle Imaging

Figures 1 and 2 show typical SEM images for the investigated HA(org)/$NaNO_3$ and HA(org)/$Ca(NO_3)_2$ particles generated from the corresponding solutions at 1:1 molar ratio. Images acquired in TE mode enable visualization of possible inclusions within individual particles whereas images acquired in SE mode are more indicative of particle surface morphology. The images show that mixing of HA(org) with either $NaNO_3$ or $Ca(NO_3)_2$ salts produces particles with nearly homogeneous internal composition. Although different components cannot be distinguished based on electron microscopy imaging, the homogeneous mixing of internal compositions is confirmed by the elemental mapping of individual particles as exemplified by Figures S1 and S2 in the supporting information. Only GA/$NaNO_3$ (1:1) particles exhibit multiple inclusions, which could be either organic sodium salt or $NaNO_3$.

The round-shaped particles with relatively smooth surfaces seen in the TE and SE mode microscopy images in Figures 1 and 2 suggest their likely noncrystalline, amorphous state. The only exception to this observation is a single, relatively large GA/$Ca(NO_3)_2$ (1:1) particle that showed a crystalline structure (see Figure 2 (bottom right)). Overall, noncrystalline particle morphologies are consistent with previous studies showing that drying of aqueous droplets can yield particles in an amorphous state for $NaNO_3$, $Ca(NO_3)_2$, and carboxylic acids investigated here [*Choi and Chan*, 2002; *Gysel et al*., 2002; *Hoffman et al*., 2004; *Krueger et al*., 2003; *Mikhailov et al*., 2009; *Peng et al*., 2001; *Wise et al*., 2003]. These particles can retain water and remain in a metastable state at very low RH, and even under vacuum conditions. Micro-FTIR analysis also supports that these particles contain condensed phase water (absorbance at about 3400 cm^{-1}) and are in viscous semisolid state (see section 3.3).

3.2. CCSEM/EDX Analysis of Individual Particles

Elemental N/Na or N/Ca ratios of individual particles were calculated from atomic fractions of N, Na, or Ca quantified by CCSEM/EDX analysis. N/Na and N/Ca data for particles in a size range of 1.0–10 μm were

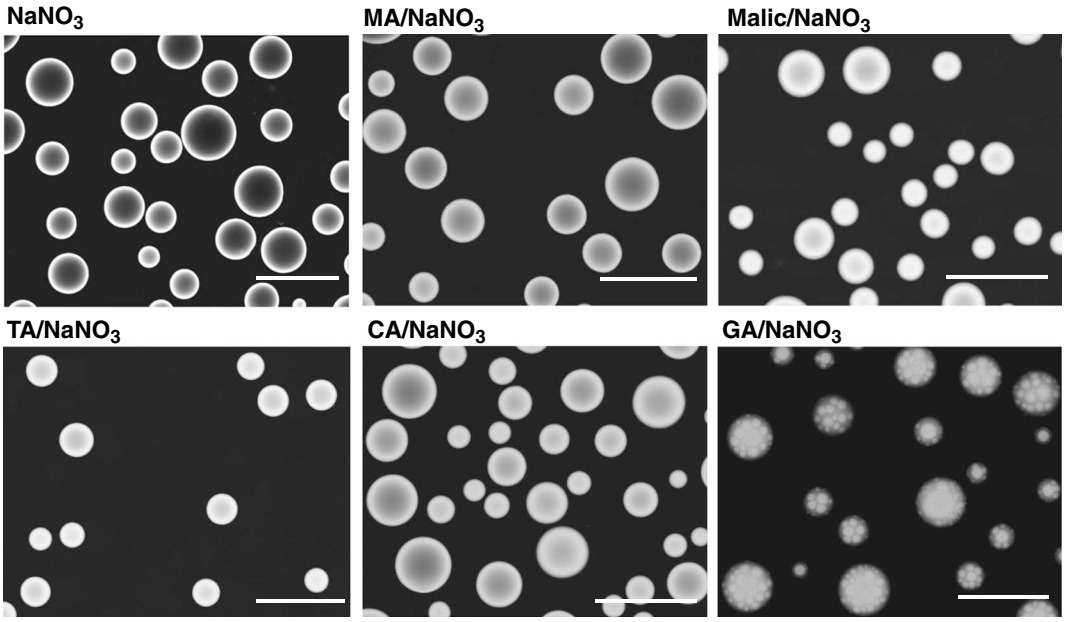

Figure 1. Characteristic SEM images of pure $NaNO_3$ particles and various mixed HA(org)/$NaNO_3$ (1:1) particles. All images were acquired in TE mode. Size bar is 10 μm for all images.

combined in 0.2 μm bins. A statistically significant number of particles (2000–10,000) were analyzed for each particle composition. Quantitative EDX analysis of particles containing $NaNO_3$, $Ca(NO_3)_2$, and their mixtures have a number of challenging issues. Intensities of characteristic EDX peaks of C, N, and O are severely affected by complex sensitivity effects (ZAF effects) related to atomic number (Z)-dependent electron scattering, absorption (A), and fluorescence (F), as well as effects of particle size and shape [*Laskin et al*., 2005b]. Furthermore, nitrate particles are susceptible to damage by the electron beam that additionally may impact measured intensities of peaks in the EDX spectra [*Hoffman et al*., 2004]. Although a few computer

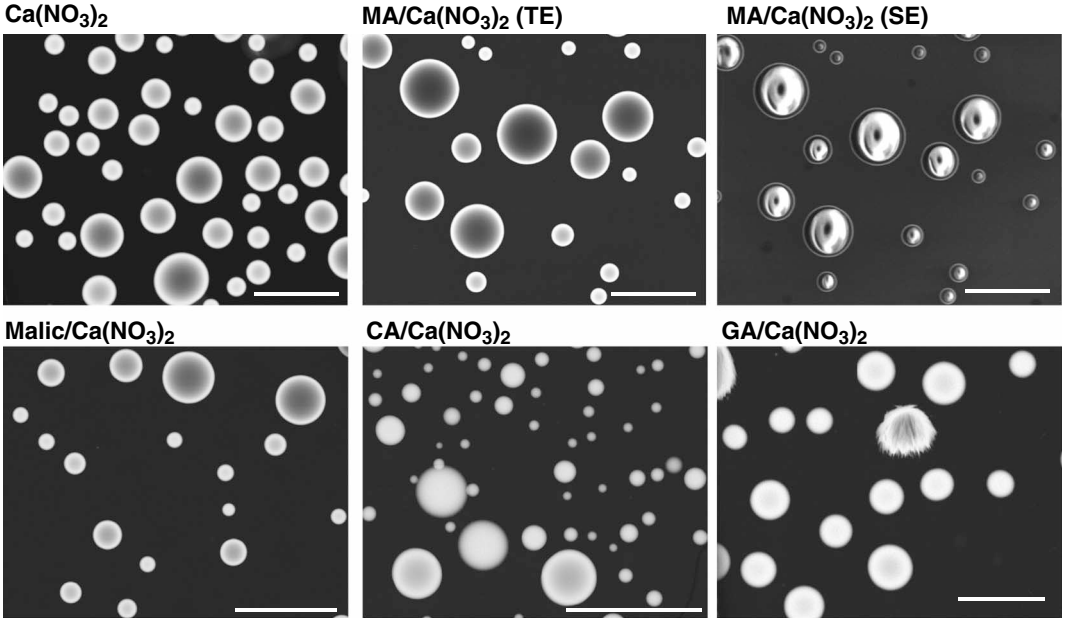

Figure 2. Characteristic SEM images of pure $Ca(NO_3)_2$ particles and various mixed HA(org)/$Ca(NO_3)_2$ (1:1) particles. Figure 2 (top right) was acquired using SE mode; all other images were acquired using TE mode. A pair of TE and SE images show the same group of MA/$Ca(NO_3)_2$ (1:1) particles. Size bar is 10 μm for all images.

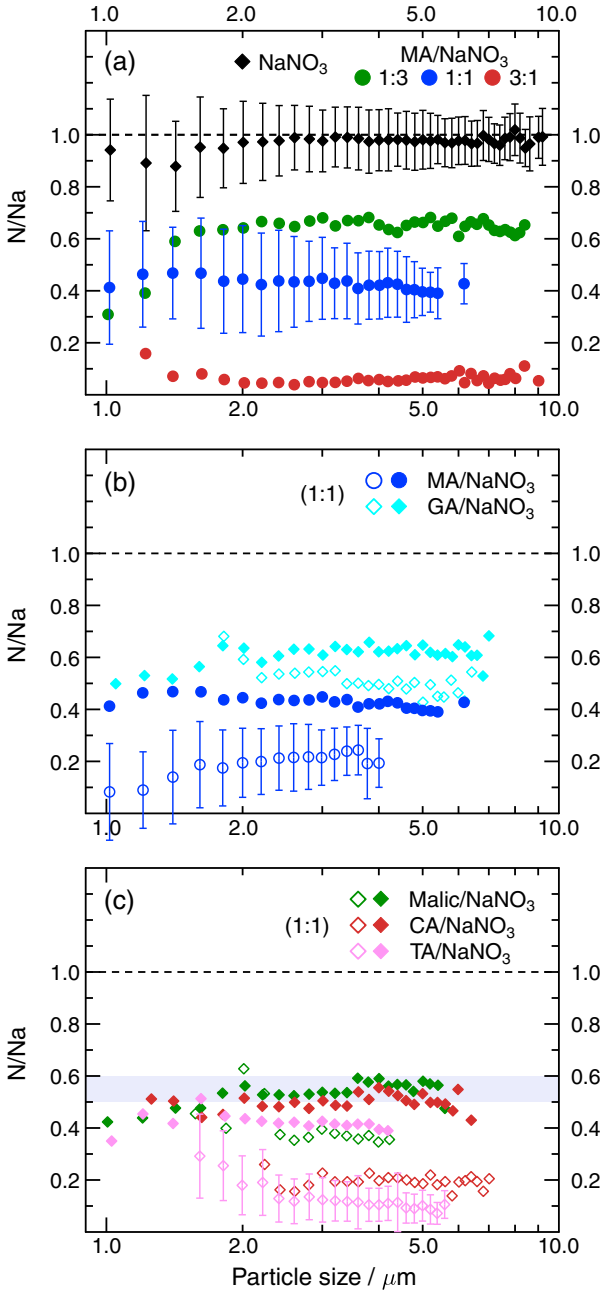

Figure 3. Mean elemental ratios of N to Na (N/Na) as a function of particle size (in diameter) for HA(org)/$NaNO_3$ particles. (a) MA/$NaNO_3$ particles generated from solutions at different molar ratios; (b, c) particles of MA, GA, Malic, CA, and TA mixed with $NaNO_3$ generated from solutions at 1:1 molar ratio. Reference data for $NaNO_3$ particles are shown as black solid diamonds. Dashed lines indicate the nominal N/Na ratio of unity if no nitrate depletion occurs. Fresh and stored particles are shown as solid and open symbols, respectively. Representative uncertainties (one standard deviation (1 SD)) are shown. Grey area in Figure 3c indicates the residual fraction of nitrate as determined by micro-FTIR measurements over CA/$NaNO_3$ (1:1) particle sample.

modeling approaches were developed to account for the sensitivity effects, these codes do not assess the beam damage effects [*Ro et al.*, 2001, 2000, 1999]. For the purpose of this study, we use measured N/Na and N/Ca ratios as indicators for residual nitrates in particles and compare their absolute values to the reference values measured for pure $NaNO_3$ and $Ca(NO_3)_2$ particles. Ratios of N/Na and N/Ca lower than the reference values indicate nitrate depletion caused by reaction (R2) between HA(org) and nitrate. Table 1 summarizes the mean N/Na and normalized N/Ca ratios with 1 standard deviation for the investigated particle samples. The ranges of ratios are shown for the particle samples that have clear size dependences.

Figure 3 shows mean ratios of N/Na measured for internally mixed HA(org)/$NaNO_3$ particles along with the reference of $NaNO_3$ particles. The N/Na reference ratios match well the nominal value of unity for nearly the entire range of particle sizes. The slightly lower N/Na values for $NaNO_3$ particles smaller than 2 μm most likely are a result of electron beam damage. N/Na ratios for all investigated HA(org)/$NaNO_3$ particles are significantly lower than the reference values indicating nitrate depletion in these particles. As shown in Figure 3a and Table 1, the N/Na ratio decreases from ~0.65 to 0.45 and to 0.1 for MA/$NaNO_3$ particles generated from 1:3, 1:1, and 3:1 mixed solutions, respectively. Nitrate was nearly completely depleted by MA in MA/$NaNO_3$ (3:1) particles. This indicates that the increase in fraction of MA within those particles enhanced nitrate depletion. In addition, the results show the nonlinear relationship between N/Na ratio (nitrate depletion) and molar ratio of MA/$NaNO_3$ (in original solution). Because the investigated organic acids are relatively weak, which means they do not fully dissociate and may have different extents of dissociation in drying aqueous particles, the H^+ concentrations in these systems and the N/Na ratios in the reacted MA/$NaNO_3$ particles are not expected to correlate linearly to the MA/$NaNO_3$ ratios in original solutions. The stored particles that were stored at 295 ± 1 K and 25%–45% RH after generation for ~4 weeks have 25% more nitrate depletions compared to the fresh particles for MA/$NaNO_3$ (1:1) particles. As shown in

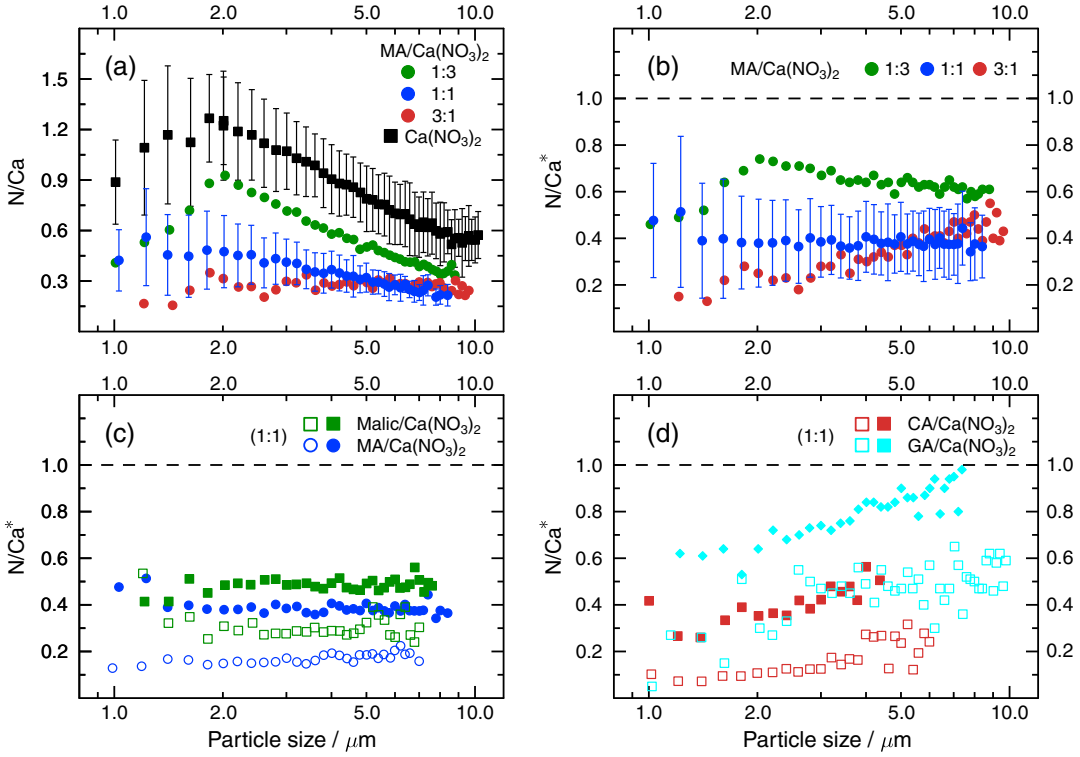

Figure 4. Mean elemental N/Ca and N/Ca* ratios (N/Ca ratios normalized to the reference N/Ca values of $Ca(NO_3)_2$ particles) for HA(org)/$Ca(NO_3)_2$ particles. (a, b) Measured N/Ca ratios and N/Ca* ratios for MA/$Ca(NO_3)_2$ (1:3, 1:1, and 3:1) particles; (c, d) N/Ca* ratios for HA(org)/$Ca(NO_3)_2$ (1:1) particles. Data for $Ca(NO_3)_2$ particles are shown as solid black squares in Figure 4a. Dashed lines indicate the N/Ca* ratio of unity if no nitrate depletion occurs. Fresh and stored particles are shown as solid and open symbols, respectively. Representative uncertainties (1 SD) are shown in Figures 4a and 4b.

Figures 3b and 3c, other organic acids exhibit different nitrate depletion potentials for the fresh (solid symbols) and stored (open symbols) HA(org)/$NaNO_3$ (1:1) particles. For fresh samples, the nitrate depletion of ~40% was observed for GA/$NaNO_3$, followed by ~45% to 50% for Malic/$NaNO_3$ and CA/$NaNO_3$, and ~55% to 60% for MA/$NaNO_3$ and TA/$NaNO_3$. About 10% to 30% of extended nitrate depletion was observed in the stored particles compared to the corresponding fresh particles. Within the experimental scatter, no significant size dependence was observed for any of the mixed HA(org)/$NaNO_3$ particles studied here.

Figure 4 shows the mean ratios of N/Ca for internally mixed HA(org)/$Ca(NO_3)_2$ particles. In the case of $Ca(NO_3)_2$ particles, the ZAF effects and beam damage are more severe than in the case of $NaNO_3$ particles for reasons that have been discussed elsewhere [*Laskin et al.*, 2005a, 2005b]. Because of the large difference between the energy of N and Ca X-ray peaks, the ZAF effects result in underpredicted values of N/Ca with an overall trend of a declining N/Ca ratio over a 1 to 10 μm particle size range. Furthermore, smaller $Ca(NO_3)_2$ particles of the submicron size are more susceptible to the electron beam-induced decomposition of nitrate, which additionally impacts underprediction of the N/Ca values. When combined, ZAF and the beam damage effects cause characteristic "rise-and-fall" tendency of the reference N/Ca values with respect to particle size, as seen in Figure 4a [*Laskin et al.*, 2005b]. As shown in Figure 4a, the reference N/Ca ratios for $Ca(NO_3)_2$ particles lie well below the nominal value of 2 because of the combined results of ZAF effects and beam damage [*Laskin et al.*, 2005b]. However, the measured N/Ca ratios for all HA(org)/$Ca(NO_3)_2$ particles were systematically lower than the N/Ca references indicating nitrate depletion by HA(org), as exemplified by the selected MA/$Ca(NO_3)_2$ particle data shown in Figure 4a. Similarly, measurements for other HA(org)/$Ca(NO_3)_2$ particles showed the same "rise-and-fall" tendency of the individual data sets over the 1 to 10 μm particle size range. To quantify the extent of the nitrate depletion in HA(org)/$Ca(NO_3)_2$ particles, the measured N/Ca ratios were normalized to the reference N/Ca values of $Ca(NO_3)_2$ particles. Therefore, the normalized mean N/Ca values (hereafter marked as N/Ca*) indicate the fraction of residual nitrate in particles. Original N/Ca data and the associated

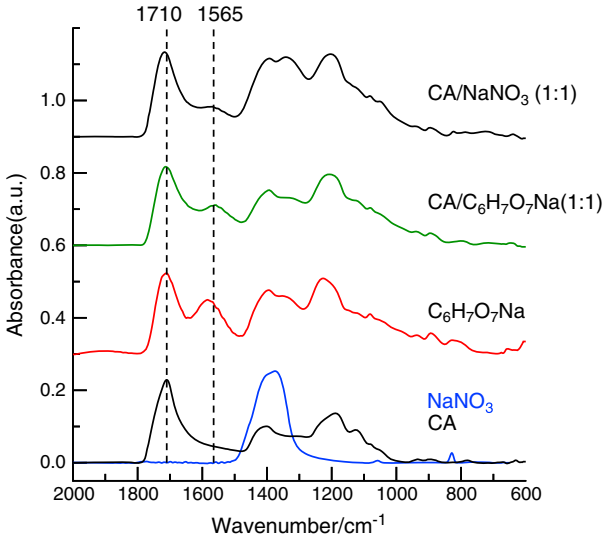

Figure 5. Micro-FTIR spectra of CA/$NaNO_3$ (1:1) particles along with the reference spectra acquired for standards of CA, $NaNO_3$, and CA/$C_6H_7O_7Na$ (1:1) particles.

normalized results for MA/$Ca(NO_3)_2$ particles are shown in Figures 4a and 4b, respectively. Figures 4c and 4d summarize the N/Ca^* ratios for HA(org)/$Ca(NO_3)_2$ (1:1) particles. In general, different extents of nitrate depletion were observed for the investigated HA(org)/$Ca(NO_3)_2$ particles. MA/$Ca(NO_3)_2$ (1:1) particles show nitrate depletion of ~60%. Nitrate depletion in MA/$Ca(NO_3)_2$ (3:1) particles are size dependent, where large particles show less depletion. MA/$Ca(NO_3)_2$ (1:3) particles have less nitrate depletion (~35%) as compared to MA/$Ca(NO_3)_2$ (1:1) and (3:1) particles. On average, nitrate depletion of 50% and 60% was observed for Malic/$Ca(NO_3)_2$ (1:1) and MA/$Ca(NO_3)_2$ (1:1) particles, respectively. No significant size dependence was observed for these two systems. For GA/Ca$(NO_3)_2$ (1:1) and CA/$Ca(NO_3)_2$ (1:1) particles, larger particles exhibited less nitrate depletion. Nitrate was further depleted by ~10% to 40% in the stored particles compared to the corresponding fresh particles as shown in Figure 4 and Table 1.

As shown in Figures 3 and 4, the stored particles have up to 30% more nitrate depletions as compared to fresh particles. As discussed in section 3.1, the investigated HA(org)/nitrate particles were in viscous semisolid state after dehydration. Because these particles retain water and remain in a metastable state at low RH, acid displacement and the release of HNO_3 into gas phase proceed gradually. This is a result of the low-diffusion coefficient of HNO_3 and organic acids in the high viscous matrix [*Koop et al.*, 2011; *Shiraiwa et al.*, 2011], in this case HA(org)/nitrate particles. Thus, the observed nitrate depletions in these stored particles can serve as the upper limits of acid displacement at 295 ± 1 K and 25%–45% RH. More depletion may occur if the particles encounter additional hydration/dehydration cycles.

3.3. Micro-FTIR Analysis

Micro-FTIR analysis was used to provide spectroscopic evidences for the organic salt formation in CA/$NaNO_3$, MA/$Ca(NO_3)_2$, and CA/$Ca(NO_3)_2$ particles. For CA/$NaNO_3$ (1:1) particles, the reaction (R2) will form monosodium citrate ($C_6H_7O_7Na$), because CA is a weak acid and may only go through first acid dissociation. This is also supported by the incomplete nitrate depletion (~50%) inferred from the CCSEM/EDX microanalysis. Figure 5 shows the spectra for CA/$NaNO_3$ (1:1) particles along with the reference spectra acquired from standards of monosodium citrate, CA, and $NaNO_3$ particles. The peak at ~1710 cm^{-1} is characteristic of the stretching mode of ν(C=O) band (COOH group) in these samples [*Cabaniss et al.*, 1998; *Ghorai et al.*, 2011; *Larkin*, 2011; *Ma et al.*, 2012]. CA/$NaNO_3$ particles post a new peak at ~1565 cm^{-1} compared to CA and $NaNO_3$ particles. This can be assigned to the out-of-plane ν(COO^-) band in the carboxylate salt (COO^- group) [*Larkin*, 2011; *Laskina et al.*, 2013; *Ma et al.*, 2012]. This peak position is the same as that detected in the standard mixture of CA/$C_6H_7O_7Na$ (1:1). The peak of COO^- functional group for pure monosodium citrate is at ~1585 cm^{-1}. This indicates that the peak experiences a red shift indicating the interaction between monosodium citrate and CA [*Laskina et al.*, 2013].

Figure 6 shows the FTIR spectra of MA/$Ca(NO_3)_2$ (1:1) and CA/$Ca(NO_3)_2$ (1:1) particles along with the reference spectra of $Ca(NO_3)_2$, MA, and CA standards. MA/$Ca(NO_3)_2$ (1:1) and CA/$Ca(NO_3)_2$ (1:1) particles post a new peak at ~1576 cm^{-1} and 1585 cm^{-1}, respectively. These newly formed peaks can also be attributed to the out-of-plane ν(COO^-) band of corresponding carboxylate salts [*Larkin*, 2011]. The peak at 1640 cm^{-1} from CA/$Ca(NO_3)_2$ (1:1) and $Ca(NO_3)_2$ particles is attributed to HOH bending of residual condensed phase water [*Liu et al.*, 2008]. The CA/$Ca(NO_3)_2$ (1:1) particles in this study were not completely dehydrated. *Peng et al.* [2001] found that MA, CA, TA, and Malic can contain water at low RH, and no crystallization was observed

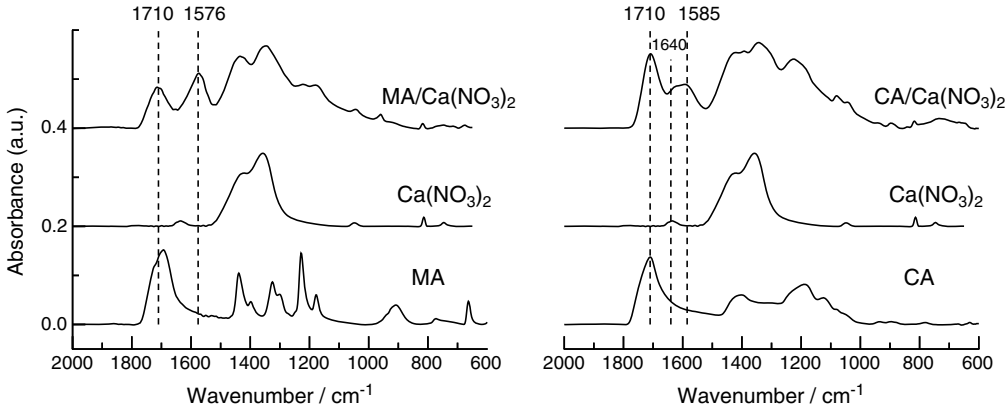

Figure 6. Micro-FTIR spectra for $MA/Ca(NO_3)_2$ (1:1) and $CA/Ca(NO_3)_2$ (1:1) particles along with the reference spectra acquired for $Ca(NO_3)_2$, MA, and CA particle standards.

even in the dehydrated particles. *Peng and Chan* [2001] and *Wu et al*. [2011] showed that some organic salts such as sodium malonate and sodium tartrate can contain water at low RH. $Ca(NO_3)_2$ particles are highly hygroscopic and deliquesces at ~12% RH [e.g., *Laskin et al*., 2005b]. From the observed particles' noncrystalline morphology inferred from SEM images and residual water detected by micro-FTIR, we suggest that the $CA/Ca(NO_3)_2$ particles were in viscous semisolid phase at low-RH conditions.

Formation of monosodium citrate in $CA/NaNO_3$ (1:1) particles was quantified from their IR spectral data using the following equation:

$$\frac{n_{p,s}}{n_{co,s}} = \frac{A_{p,s}/\sigma_p}{A_{co,s}/\sigma_{co}} = \frac{\sigma_{co}}{\sigma_p} \times \frac{A_{p,s}}{A_{co,s}}, \quad (1)$$

where $n_{p,s}$ and $n_{co,s}$ are the moles of monosodium citrate product and CA, respectively; $A_{p,s}$ and $A_{co,s}$ are the integrated absorbance; and σ_{co} and σ_p are the integrated cross sections of ν(C=O) and $\nu(COO^-)$ bands, respectively. The ratio of σ_p to σ_{co} was determined from the deconvoluted reference spectrum of $CA/C_6H_7O_7Na$ (1:1) particle standard. For $CA/NaNO_3$ (1:1) particles, the fraction of monosodium citrate (X_p) of ~0.45 ± 0.05 was determined using the following equation:

$$\frac{n_{p,s}}{n_{co,s}} = \frac{X_p}{(1 - X_p)}. \quad (2)$$

When converted to N/Na ratio, $X_p = 0.45 \pm 0.05$ corresponds to the ratio of 0.55 ± 0.05, which is consistent with the results of CCSEM/EDX analysis shown in Figure 3c.

3.4. Driving Forces of Reactions

The CCSEM/EDX microanalysis and micro-FTIR spectroscopy confirm the nitrate depletion and the formation of organic salts in a set of investigated HA(org)/nitrate particles following reaction (R2). In our previous study, we demonstrated that the extent of chloride depletion in different HA(org)/NaCl particles is controlled by the gas phase release of HCl(g) that shifts gas-particle equilibrium of reaction (R1) toward its products [*Laskin et al*., 2012]. The same arguments hold for reaction (R2) and the case of mixed HA(org)/nitrate particles. In general, the equilibrium conditions of these reactions for diluted aqueous particles are governed by the differences in acidity and volatility of HA(org) versus those of HNO_3.

Table 2 lists the acid dissociation constants (K_{a1}) and Henry's law constants (K_H) for the acids discussed in this study along with the corresponding ratios of $\frac{K_{a,HNO3}}{K_{a1,HA(org)}}$ and $\frac{K_{H,HA(org)}}{K_{H,HNO3}}$ calculated for each HA(org). Differences in relative acidities (dissociations) of HNO_3 and HA(org), $\frac{K_{a,HNO3}}{K_{a1,HA(org)}}$, indicate that equilibrium concentration of undissociated organic acids will be a factor of 10^4–10^5 higher than that of the undissociated HNO_3, shifting equilibrium of reaction (R2) to the left. On the other hand, differences in the corresponding K_H values $\left(\frac{K_{H,HA(org)}}{K_{H,HNO3}}\right)$ suggest that the HNO_3 gas phase concentration will exceed HA(org) gas phase concentration by a

Table 2. Physicochemical Properties of Acids Discussed in This Study Including Molecular Formula, Molar Mass, Acid Dissociation Constant (Acidity Constant, K_{a1}), and Henry's Law Constant (K_H)[a]

Acids	Molecular Formula	Molar Mass (g mol^{-1})	Acidity Constant, K_{a1}[b]	Henry's Law Constant, K_H[c], (M/atm)	$\frac{K_{a,HNO3}}{K_{a1,HA(org)}}$	$\frac{K_{H,HA(org)}}{K_{H,HNO3}}$
Hydrochloric	HCl	36.46	$>1\times10^{7}$	$<2\times10^{-1}$		
Nitric	HNO_3	63.01	$>2\times10^{1}$	$>2\times10^{5}$		
Glutaric (GA)	$C_5H_8O_4$	132.12	4.8×10^{-5}	$(0.35–3.3)\times10^{9}$	4.2×10^{5}	$(0.2–1.7)\times10^{4}$
Malonic (MA)	$C_3H_4O_4$	104.06	1.5×10^{-3}	$(0.26–3.3)\times10^{10}$	1.3×10^{4}	$(0.1–1.7)\times10^{5}$
Malic	$C_4H_6O_5$	134.09	3.9×10^{-4}	3.5×10^{10}	5.1×10^{4}	1.8×10^{5}
Tartaric (TA)	$C_4H_6O_6$	150.09	1.0×10^{-3}	1.5×10^{10}	2.0×10^{4}	7.5×10^{4}
Citric (CA)	$C_6H_8O_7$	192.12	8.4×10^{-4}	6.5×10^{10}	2.4×10^{4}	3.3×10^{5}

[a] K_{a1} ratio of nitric to organic acid $\left(\frac{K_{a,HNO3}}{K_{a1,HA(org)}}\right)$ and K_H ratio of organic to nitric acid $\left(\frac{K_{H,HA(org)}}{K_{H,HNO3}}\right)$ are listed.

[b] Data from *Haynes and Lide* [2011].

[c] Data from *Bilde et al.* [2003], *Booth et al.* [2010], *Cappa et al.* [2007], *Compernolle and Müller* [2013], *Ribeiro da Silva et al.* [1999], *Salo et al.* [2010], and *Soonsin et al.* [2010]. The range of K_H values for MA and GA is compiled from the listed references.

comparable factor of ~10^5. Notably, with the exception of GA, for all other HA(org) species the gas phase excess of HNO_3 is larger than its shortage in the aqueous phase. Therefore, upon drying of particles, the equilibrium of reaction (R2) will be gradually changed and shifted to the right by the continuous degassing of HNO_3 to the point where concentrations of "reactants" and "products" in the condensed phase would become comparable. Calculated ratios of $\frac{K_{H,HA(org)}}{K_{H,HNO3}} / \frac{K_{a,HNO3}}{K_{a1,HA(org)}}$ can be used to compare the differences in the corresponding K_H and K_{a1} of HNO_3 and HA(org) and assess plausibility of reaction (R2). Higher $\frac{K_{H,HA(org)}}{K_{H,HNO3}} / \frac{K_{a,HNO3}}{K_{a1,HA(org)}}$ values indicate greater tendency for HNO_3 evaporation and higher extent of nitrate depletion. As shown in Figure 7, the $\frac{K_{H,HA(org)}}{K_{H,HNO3}} / \frac{K_{a,HNO3}}{K_{a1,HA(org)}}$ value of 4.2×10^{-3} to 4.0×10^{-2} for GA is more than 2 orders of magnitude lower than those values ($1–1.4\times10^{1}$) for other HA(org), so GA showed the least nitrate depletion among the investigated HA(org). The stored particles also showed a similar trend (Figure S3). *Saxena and Hildemann* [1996] reported that the estimated K_H of Malic, TA, and CA could be 2×10^{13}, 1×10^{18}, and 2×10^{18} M/atm, respectively, which is several orders of magnitude higher than the values used in Table 2. This indicates that estimated gas phase excess of HNO_3 can be several orders of magnitude higher than its condensed phase shortage for systems of Malic, TA, and CA mixed with nitrate. Therefore, a greater shift of the reaction (R2) equilibrium to the right would be expected for $NaNO_3$ and $Ca(NO_3)_2$ particles reacted with MA, Malic, TA, and CA, while their reactivity with GA would be less noticeable. This is consistent with our CCSEM/EDX results showing similar nitrate depletion in both $NaNO_3$ and $Ca(NO_3)_2$ particles mixed with CA, MA, Malic, and TA, and substantially lesser effect in those particles mixed with GA (see Table 1).

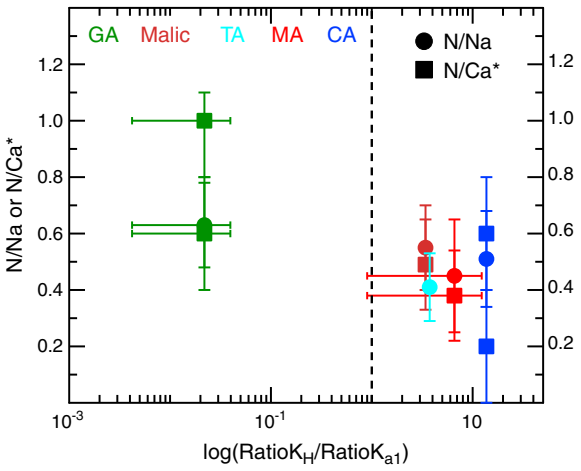

Figure 7. Ratios of N/Na (circle) and N/Ca* (square) observed in mixed HA(org)/nitrate (1:1) fresh particles as a function of $\frac{K_{H,HA(org)}}{K_{H,HNO3}} / \frac{K_{a,HNO3}}{K_{a1,HA(org)}}$ (i.e., RatioK_H/RatioK_{a1}). Dashed lines show the $\frac{K_{H,HA(org)}}{K_{H,HNO3}} / \frac{K_{a,HNO3}}{K_{a1,HA(org)}}$ value of 1. Two data points for CA/$Ca(NO_3)_2$ and GA/ $Ca(NO_3)_2$ represent the range of N/Ca*. Green, brown, cyan, red, and blue represent mixed nitrate with GA, Malic, TA, MA, and CA, respectively. Error bars in *x* axis for GA and MA indicate the ranges of literature-reported data. Error bars in *y* axis represent 1 standard deviation listed in Table 1.

Interestingly, we were unable to produce and study individual particles generated from the mixture of TA and $Ca(NO_3)_2$ solutions because of the very low solubility of calcium tartrate in water, which is below 0.36 g/L at 20°C (0.002 *M*) [*Seidell*, 1919]. Therefore, bulk calcium tartrate product precipitated immediately when 0.5 *M* solutions of TA and $Ca(NO_3)_2$ were mixed together. This indicates that low solubility of

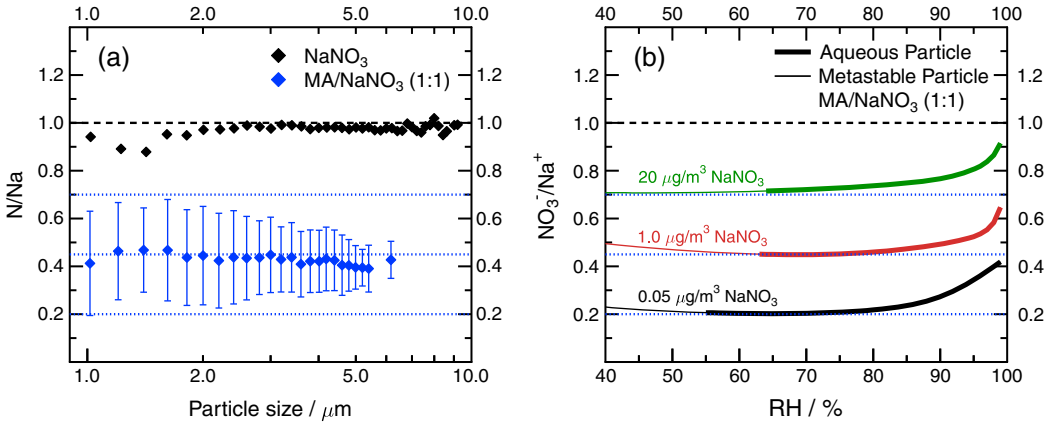

Figure 8. (a) Mean N/Na ratios as a function of particle size determined by CCSEM/EDX analysis for dried MA/$NaNO_3$ (1:1) particles. Error bars represent 1 standard deviation (1 SD). Dotted lines indicate the range of N/Na ratio (mean ± 1 SD). (b) Results of E-AIM calculation predicting condensed phase NO_3^-(aq)/Na^+ ratios as a function of RH at gas/particle equilibrium for aqueous (thick lines) and metastable (thin lines) of MA/$NaNO_3$ (1:1) particles. Legends indicate airborne $NaNO_3$ concentrations adjusted to match measured N/Na ratios shown in Figure 8a.

certain organic salts would have an additional effect on driving the reactions between HA(org) and nitrate in atmospheric aerosols.

As shown in Figures 3 and 4, the extent of nitrate depletion in CA/$Ca(NO_3)_2$ and GA/$Ca(NO_3)_2$ particles exhibits significant size dependence, while nitrate depletion in other HA(org)/$Ca(NO_3)_2$ particles is invariant of particle size. It is possible that for the later HA(org)/$Ca(NO_3)_2$ systems, the particle phase diffusion of HNO_3 is fast enough that particle size has no significant effect on the HNO_3 transport from particle to gas phase during the dehydration processes. In contrast, for CA/$Ca(NO_3)_2$ and GA/$Ca(NO_3)_2$ particles, particle phase diffusion of HNO_3 is likely slower to the point that particle size limits the HNO_3 transport throughout the particle and its gas phase partitioning at low RH. The reason for that could be that CA/$Ca(NO_3)_2$ and GA/$Ca(NO_3)_2$ particles become more viscous or semisolid as result of fast dehydration in the diffusion dryer [*Koop et al.*, 2011; *Shiraiwa et al.*, 2011] and lower solubility of associated calcium salts and their possible crystallization.

4. Atmospheric Implications

Although the data presented here are for 1.0 to 10 μm particles, the gas/particle partitioning through reaction (R2) would occur even faster in smaller particles in which greater nitrate depletion may be expected. To estimate the extent of this reaction at ambient conditions, partitioning among gas, liquid, and solid phases for some of the investigated aerosol systems was calculated using the E-AIM model [*Clegg and Seinfeld*, 2006a, 2006b]. Specifically, Model III of E-AIM at 1 atm ambient pressure and 298.15 K in a closed 1 m^3 air parcel was used with standard UNIFAC (UNIversal Functional Group Activity Coefficients) parameters for HA(org).

Figure 8 shows NO_3^-(aq)/Na^+ equilibrium ratios as a function of RH for MA/$NaNO_3$ (1:1) for deliquesced aqueous (thick lines) microdroplets and particles in metastable aqueous form (thin lines) calculated when formation of solid phases was disabled in the model. Intentionally, we selected the input value of MA/$NaNO_3$ (1:1) aerosol concentration to be such that the calculated NO_3^-(aq)/Na^+ ratio would match the measured N/Na ratio of 0.45 in corresponding CCSEM/EDX analysis (Figure 8b). Figure 8a shows that NO_3^-(aq)/Na^+ ratio of 0.45 would be expected over the range of 55%–80% RH if the model is initialized with an input of 1.0 μg/m^3 for airborne $NaNO_3$ concentration (1.18×10^{-2} μmol/m^3) mixed with MA at 1:1 molar ratio. The upper and lower limits of measured N/Na ratio set by the error bars (0.45 ± 0.20) can be simulated using an input of 20 and 0.05 μg/m^3 for airborne $NaNO_3$ concentrations, respectively, which are well within the range of common nitrate mass loadings in typical atmospheric environments [e.g., *Adams et al.*, 1999; *Bauer et al.*, 2007].

Table 3 shows the range of airborne nitrate concentrations used as E-AIM model input to match corresponding levels of nitrate depletion observed in dry MA/$NaNO_3$, Malic/$NaNO_3$, and GA/$NaNO_3$ particles. The calculated NO_3^-(aq)/Na^+ ratios from the E-AIM model between 40% and 80% RH (colored lines in

Table 3. Estimated Range of Airborne $NaNO_3$ Concentrations From E-AIM Model Calculation Where Nitrate Depletion at Low RH (~40%–80%) Can be Expected at the Same Levels (Indicated by N/Na) as Those Measured for Selected HA(org)/$NaNO_3$ Particles[a]

Organic Acid, HA(org)	Molar Ratio HA(org)/$NaNO_3$	Extent of Nitrate Depletion in Dry Particles: N/Na (mean ± 1 SD)	Airborne $NaNO_3$ Concentrations Required to Account for the Corresponding Nitrate Depletion ($\mu g/m^3$)			Range of Potential HNO_3(g) Production ($\mu g/m^3$)		
			Upper Limit	Mean	Lower Limit	Upper Limit	Mean	Lower Limit
MA	1:3	0.65 ± 0.20	50	1	0.05	16.7	0.33	0.02
	1:1	0.45 ± 0.20	20	1	0.05	8	0.4	0.02
	3:1	0.10 ± 0.10	0.05	0.01	0.001	0.03	0.01	~0
Malic	1:1	0.55 ± 0.15	12	5	2	4.4	1.9	0.9
GA	1:1	0.63 ± 0.15	0.5	0.05	0.01	0.1	0.01	~0

[a]Range of potential HNO_3(g) production is also reported. Upper and lower limits correspond to mean + 1 SD and mean − 1 SD of N/Na ratio, respectively.

Figure 8b) match the experimentally determined N/Na ratios (dotted lines in Figure 8a). The upper and lower limits of airborne nitrate concentrations correspond to mean + 1 standard deviation (SD) and mean − 1 SD of N/Na ratio, respectively. Because these calculations were done for a constant volume system, higher-nitrate concentration results in lower nitrate depletion for the same HA(org)/$NaNO_3$ particles shown in Figure 8b. During their atmospheric aging, sea salt and calcite components of mineral dust can be fully converted into nitrate particles [e.g., *Abbatt et al*., 2012; *Laskin et al*., 2005a]. Considering typical airborne sea salt concentrations of 1–1000 $\mu g/m^3$ in the atmosphere [*Lewis and Schwartz*, 2004], we conclude that all nitrate concentrations listed in Table 3 are atmospherically relevant. E-AIM model calculations with an input of MA/NH_4NO_3 at 1:1 molar ratio (with 10 $\mu g/m^3$ NH_4NO_3) show that the majority of NH_4NO_3 will be in the gas phase below 80% RH. Thus, the acid displacement by MA may have no significant impact in terms of overall nitrate partitioning in the MA/NH_3/HNO_3 aerosol system.

The corresponding gas phase concentrations of HNO_3(g) for these investigated systems range from 0 to 16.7 $\mu g/m^3$ and are listed in Table 3. These concentrations are in the same order of magnitude as those reported in field studies of atmospheric HNO_3(g) at different geographic locations [e.g., *Adon et al*., 2010; *Day et al*., 2009; *Fischer et al*., 2006; *Hu et al*., 2008; *Lefer et al*., 1999; *Li et al*., 2012; *Morino et al*., 2006]. For example, *Fischer et al*. [2006] measured mean HNO_3 concentrations of ~2.3 $\mu g/m^3$ with a maximum of 21 $\mu g/m^3$ in the New England coastal atmosphere during summer time. In that study, the elevated HNO_3(g) to particulate phase nitrate ratio of 2–6 were reported during the episodes of urban plumes, which likely would have been impacted by higher concentrations of organics. Previous studies have shown that in Mexico City secondary oxygenated organics [*Aiken et al*., 2009] and organic acids [*Knopf et al*., 2010; *Moffet et al*., 2010; *Stone et al*., 2010] often mix internally with nitrate, such as $NaNO_3$ and $Zn(NO_3)_2$ [*Aiken et al*., 2009; *Moffet et al*., 2008]. Low molecular weight carboxylic acids can be up to 4 $\mu g/m^3$ [*Stone et al*., 2010]. If the proposed reaction occurred and nitrate depletion was similar to that in mixed MA/$NaNO_3$ (1:1) particles with $NaNO_3$ of 1 $\mu m/m^3$ (Table 3), ~0.4 $\mu m/m^3$ HNO_3(g) would be produced. This would have accounted for 16% of measured mean HNO_3(g) concentration at noon time (~1 ppb; i.e., 2.58 $\mu m/m^3$) [*Zheng et al*., 2008]. *Zheng et al*. [2008] also showed that ~23% HNO_3 production could not be balanced after considering the photochemical production, deposition, and losses. Thus, the production of HNO_3 from the proposed reactions may contribute significantly to the HNO_3 atmospheric budget.

Results of E-AIM calculations suggest that for HA(org)/$NaNO_3$ particles gas/particle partitioning through reaction (R2) might be significant over a very wide range of RH <80% (see Figure 8b). As shown in Figure 8b, the NO_3^-(aq)/Na^+ ratios for aerosol systems with low MA/$NaNO_3$ concentrations (red and black lines) are significantly lower than 1 even at RH close to 100%. This implies that HA(org) can possibly deplete nitrate not only during substantial dehydration but also during cloud processing. Reactions between various HA(org) and nitrate can release gaseous HNO_3 and produce organic salts, which would become a significant component of mixed particles. The current version of the E-AIM model only considers formation of solid organic acids and inorganics separately and does not include solid organic salts formation. Formation and precipitation of organic salts need to be considered in future modeling efforts for better estimation of the chemical composition of complex organic/nitrate/chloride particles, especially at low-RH conditions. Formation of organic salts from reactions (R1) and (R2) may alter particles' physical properties, such as

hygroscopicity and refractive index. For instance, a few studies have shown that organic salts including sodium malonate and sodium tartrate are more hygroscopic than their corresponding acids and are comparable to typical hygroscopic inorganic salts [*Peng and Chan*, 2001; *Wu et al*., 2011].

The acid displacement reaction (R2) provides a recycling mechanism of HNO_3. Release of gaseous HNO_3 from reaction and its repartitioning on surfaces of other particles and environmental surfaces [e.g., *Baergen and Donaldson*, 2012] may have significant impacts and consequences for atmospheric chemistry and environments. The released HNO_3 could react with ammonia (NH_3) and form ammonium nitrate [*Seinfeld and Pandis*, 1998]. The enhanced gas phase HNO_3 would also affect nighttime nitrogen chemistry [e.g., *Brown and Stutz*, 2012]. Additional sinks of HNO_3, such as heterogeneous reactions with sea salt, mineral dust, soot [*Loukhovitskaya et al*., 2013; *Salgado Munoz and Rossi*, 2002], and organic aerosols [e.g., *Moussa et al*., 2013; *Ziemba et al*., 2010], will extend the reaction between HA(org) and nitrate particles. For coastal and urban regions where HNO_3, sea salt/mineral dust, and HA(org) are abundant, HNO_3 can first react with sea salt and mineral dust particles and form highly hydroscopic nitrates. When these nitrate particles interact or mix with HA(org), HNO_3 can be re-released as a result of acid displacement and then continues to react with sea salt and mineral dust.

On the other hand, substantial presence of ammonia or amines in the particle content can counter balance reactions (R1) and (R2) through the competing consumption of organic acids leading to formation of ammonium/aminium salts and amides following reactions (R3) shown below [*Qiu and Zhang*, 2013; *Rehbein et al*., 2011; *Zhang et al*., 2012].

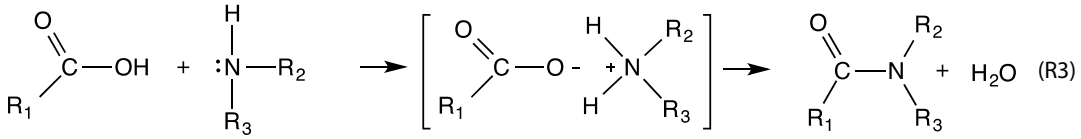

These reactions will reduce concentration of protons available for the acid displacement reactions ((R1) and (R2)) inhibiting yields and gas phase partitioning of the HNO_3 and HCl products. Furthermore, in an atmospheric environment, hydration and dehydration cycles of particles may cause either partial crystallization of particle components [*Ault et al*., 2013; *Liu et al*., 2011] or liquid-liquid phase separations [*You et al*., 2012] that in turn would impact internal distribution of various components with inherent effects on particle reactivity and gas-particle partitioning of the reaction products. The influence of all these factors on the potential recycling of HNO_3 through (R2) will be an interesting topic for future investigations following the case study presented here.

5. Conclusions

Nitrate depletion and formation of organic salts in atmospherically relevant particles composed of water-soluble organic acids (HA(org)) and nitrate (i.e., $NaNO_3$ and $Ca(NO_3)_2$) were investigated using CCSEM/EDX analysis of a statistically significant number of individual particles and micro-FTIR analysis of ensembles of a few hundred particles. The results show that HA(org) can react with nitrate resulting in the release of gaseous HNO_3 and formation of organic salts during the dehydration process. Among the investigated HA(org) species, malonic and tartaric acids show greatest nitrate depletion (~55%–60%) followed by malic and citric acids (~45%–55%) and glutaric acid (~37%) for $NaNO_3$. Higher HA(org) content in HA(org)/nitrate particles results in greater nitrate depletion. No significant size dependence was observed for the investigated 1–10 μm size HA(org)/$NaNO_3$ particles. Similar nitrate depletions were observed for HA(org)/$Ca(NO_3)_2$ particles except for those with glutaric and citric acids which showed slight size dependence. Greater nitrate depletion was observed in all investigated samples when they were stored at low-RH conditions ($<$45% at room temperature). This is most likely a result of slow reaction and diffusion in the viscous semisolid particles. The results from micro-FTIR analysis confirm the formation of organic salts and are consistent with CCSEM/EDX analysis in nitrate depletion.

The nitrate depletion and organic salt formation are attributed to acid displacement of nitrate with HA(org) through gas-particle reactive processes driven by the evaporation of HNO_3 into the gas phase as particles dehydrate. It is reasonable to expect that similar reactive reactions will also apply for other mixtures of

nitrates with water-soluble organic acids. Similar reactions and processes applied to HA(org)/NaCl particles and different HA(org) have shown various impacts on the chloride depletion levels [*Ghorai et al*., 2014; *Laskin et al*., 2012]. Relevant airborne nitrate concentrations that might be subjects for these reactions are estimated using a thermodynamic model (E-AIM). Those estimated concentrations are well within the typical range of nitrate mass loadings reported for various atmospheric environments. The release of HNO_3(g) from these reactions could have considerable effects on the nitrate-nitric acid partitioning and its atmospheric budget. The reported reaction suggests a potential mechanism of HNO_3 recycling that would affect the related gas and heterogeneous chemistry in the atmosphere. The resulting organic salts can contribute to a significant fraction of particle content and may change the particles' chemical and physical properties. These effects of the reactive gas/particle partitioning in mixed HA(org)/$NaNO_3$/NaCl particles were largely overlooked by previous work; therefore, they need to be considered in future field, laboratory, and modeling studies.

Acknowledgments

The authors acknowledge support from the Chemical Imaging Initiative of the Laboratory Directed Research and Development program at Pacific Northwest National Laboratory (PNNL). The CCSEM/EDX and micro-FTIR particle analysis was performed in the Environmental Molecular Sciences Laboratory (EMSL), a national scientific user facility sponsored by the U.S. Department of Energy Office of Biological and Environmental Research and located at PNNL. PNNL is operated for DOE by Battelle Memorial Institute under contract DE-AC05-76RL0.

References

Abbatt, J. P. D., A. K. Y. Lee, and J. A. Thornton (2012), Quantifying trace gas uptake to tropospheric aerosol: Recent advances and remaining challenges, *Chem. Soc. Rev.*, *41*(19), 6555–6581, doi:10.1039/C2CS35052A.

Adams, P. J., J. H. Seinfeld, and D. M. Koch (1999), Global concentrations of tropospheric sulfate, nitrate, and ammonium aerosol simulated in a general circulation model, *J. Geophys. Res.*, *104*(D11), 13,791–13,823, doi:10.1029/1999JD900083.

Adon, M., et al. (2010), Long term measurements of sulfur dioxide, nitrogen dioxide, ammonia, nitric acid and ozone in Africa using passive samplers, *Atmos. Chem. Phys.*, *10*(15), 7467–7487, doi:10.5194/acp-10-7467-2010.

Aiken, A. C., et al. (2009), Mexico City aerosol analysis during MILAGRO using high resolution aerosol mass spectrometry at the urban supersite (T0)—Part 1: Fine particle composition and organic source apportionment, *Atmos. Chem. Phys.*, *9*(17), 6633–6653, doi:10.5194/acp-9-6633-2009.

Albrecht, B. A. (1989), Aerosols, cloud microphysics, and fractional cloudiness, *Science*, *245*(4923), 1227–1230, doi:10.1126/science.245.4923.1227.

Andreae, M. O., and P. J. Crutzen (1997), Atmospheric aerosols: Biogeochemical sources and role in atmospheric chemistry, *Science*, *276*(5315), 1052–1058, doi:10.1126/science.276.5315.1052.

Ault, A. P., T. L. Guasco, O. S. Ryder, J. Baltrusaitis, L. A. Cuadra-Rodriguez, D. B. Collins, M. J. Ruppel, T. H. Bertram, K. A. Prather, and V. H. Grassian (2013), Inside versus outside: Ion redistribution in nitric acid reacted sea spray aerosol particles as determined by single particle analysis, *J. Am. Chem. Soc.*, *135*(39), 14,528–14,531, doi:10.1021/ja407117x.

Baergen, A. M., and D. J. Donaldson (2012), Photochemical renoxification of nitric acid on real urban grime, *Environ. Sci. Technol.*, *47*(2), 815–820, doi:10.1021/es3037862.

Baker, M. B. (1997), Cloud microphysics and climate, *Science*, *276*(5315), 1072–1078, doi:10.1126/science.276.5315.1072.

Baltrusaitis, J., and V. H. Grassian (2012), Atomic force microscopy and X-ray photoelectron spectroscopy study of NO_2 reactions on $CaCO_3$ surfaces in humid environments, *J. Phys. Chem. A*, *116*(36), 9001–9009, doi:10.1021/jp305122d.

Bauer, S. E., D. Koch, N. Unger, S. M. Metzger, D. T. Shindell, and D. G. Streets (2007), Nitrate aerosols today and in 2030: A global simulation including aerosols and tropospheric ozone, *Atmos. Chem. Phys.*, *7*(19), 5043–5059, doi:10.5194/acp-7-5043-2007.

Bilde, M., B. Svenningsson, J. Mønster, and T. Rosenørn (2003), Even-odd alternation of evaporation rates and vapor pressures of C3-C9 dicarboxylic acid aerosols, *Environ. Sci. Technol.*, *37*(7), 1371–1378, doi:10.1021/es0201810.

Booth, A. M., M. H. Barley, D. O. Topping, G. McFiggans, A. Garforth, and C. J. Percival (2010), Solid state and sub-cooled liquid vapour pressures of substituted dicarboxylic acids using Knudsen Effusion Mass Spectrometry (KEMS) and Differential Scanning Calorimetry, *Atmos. Chem. Phys.*, *10*(10), 4879–4892, doi:10.5194/acp-10-4879-2010.

Brown, S. S., and J. Stutz (2012), Nighttime radical observations and chemistry, *Chem. Soc. Rev.*, *41*(19), 6405–6447, doi:10.1039/C2CS35181A.

Cabaniss, S. E., J. A. Leenheer, and I. F. McVey (1998), Aqueous infrared carboxylate absorbances: Aliphatic di-acids, *Spectrochim. Acta A*, *54*(3), 449–458.

Cain, J. P., P. L. Gassman, H. Wang, and A. Laskin (2010), Micro-FTIR study of soot chemical composition—Evidence of aliphatic hydrocarbons on nascent soot surfaces, *Phys. Chem. Chem. Phys.*, *12*(20), 5206–5218, doi:10.1039/b924344e.

Cappa, C. D., E. R. Lovejoy, and A. R. Ravishankara (2007), Determination of evaporation rates and vapor pressures of very low volatility compounds: A study of the C4–C10 and C12 dicarboxylic acids, *J. Phys. Chem. A*, *111*(16), 3099–3109, doi:10.1021/jp068686q.

Chebbi, A., and P. Carlier (1996), Carboxylic acids in the troposphere, occurrence, sources, and sinks: A review, *Atmos. Environ.*, *30*(24), 4233–4249.

Chen, H., J. G. Navea, M. A. Young, and V. H. Grassian (2011), Heterogeneous photochemistry of trace atmospheric gases with components of mineral dust aerosol, *J. Phys. Chem. A*, *115*(4), 490–499, doi:10.1021/jp110164j.

Choi, M. Y., and C. K. Chan (2002), Continuous measurements of the water activities of aqueous droplets of water-soluble organic compounds, *J. Phys. Chem. A*, *106*(18), 4566–4572, doi:10.1021/jp013875o.

Clegg, S. L., and J. H. Seinfeld (2006a), Thermodynamic models of aqueous solutions containing inorganic electrolytes and dicarboxylic acids at 298.15 K. I. The acids as non-dissociating components, *J. Phys. Chem. A*, *110*, 5692–5717.

Clegg, S. L., and J. H. Seinfeld (2006b), Thermodynamic models of aqueous solutions containing inorganic electrolytes and dicarboxylic acids at 298.15 K. II. Systems including dissociation equilibria, *J. Phys. Chem. A*, *110*, 5718–5734.

Compernolle, S., and J. F. Müller (2013), Henry's law constants of diacids and hydroxypolyacids: Recommended values, *Atmos. Chem. Phys. Discuss.*, *13*(9), 25,125–25,156, doi:10.5194/acpd-13-25125-2013.

Day, D. A., D. K. Farmer, A. H. Goldstein, P. J. Wooldridge, C. Minejima, and R. C. Cohen (2009), Observations of NOx, SPNs, SANs, and HNO_3 at a rural site in the California Sierra Nevada mountains: Summertime diurnal cycles, *Atmos. Chem. Phys.*, *9*(14), 4879–4896, doi:10.5194/acp-9-4879-2009.

Finlayson-Pitts, B. J. (2003), The tropospheric chemistry of sea salt: A molecular-level view of the chemistry of NaCl and NaBr, *Chem. Rev.*, *103*(12), 4801–4822, doi:10.1021/cr020653t.

Fiore, A. M., et al. (2012), Global air quality and climate, *Chem. Soc. Rev.*, *41*(19), 6663–6683, doi:10.1039/C2CS35095E.

Fischer, E., A. Pszenny, W. Keene, J. Maben, A. Smith, A. Stohl, and R. Talbot (2006), Nitric acid phase partitioning and cycling in the New England coastal atmosphere, *J. Geophys. Res.*, *111*, D23S09, doi:10.1029/2006JD007328.

Forster, P., V. Ramaswamy, P. Artaxo, T. Berntsen, and R. Betts (2007), Climate change 2007: The physical science basis, in *Contribution of Working Group I to the Fourth Assessment Report of the Intergovernmental Panel on Climate Change*, edited by S. Solomon et al., pp. 996, Cambridge Univ. Press, Cambridge, U. K., and New York.

Gard, E. E., et al. (1998), Direct observation of heterogeneous chemistry in the atmosphere, *Science*, *279*(5354), 1184–1187, doi:10.1126/science.279.5354.1184.

Ghorai, S., A. Laskin, and A. V. Tivanski (2011), Spectroscopic evidence of keto–enol tautomerism in deliquesced malonic acid particles, *J. Phys. Chem. A*, *115*(17), 4373–4380, doi:10.1021/jp112360x.

Ghorai, S., B.-B. Wang, A. V. Tivanski, and A. Laskin (2014), Hygroscopic properties of internally mixed particles composed of NaCl and water soluble organic acids, *Environ. Sci. Technol.*, *48*(4), 2234–2241, doi:10.1021/es404727u.

Gibson, E. R., P. K. Hudson, and V. H. Grassian (2006), Physicochemical properties of nitrate aerosols: Implications for the atmosphere, *J. Phys. Chem. A*, *110*(42), 11,785–11,799, doi:10.1021/jp063821k.

Gysel, M., E. Weingartner, and U. Baltensperger (2002), Hygroscopicity of aerosol particles at low temperatures. 2. Theoretical and experimental hygroscopic properties of laboratory generated aerosols, *Environ. Sci. Technol.*, *36*(1), 63–68, doi:10.1021/es010055g.

Haynes, W. M., and D. R. Lide (2011), *CRC Handbook of Chemistry and Physics*, 2nd ed., vol. 9, CRC, Boca Raton, Fla.

Heal, M. R., P. Kumar, and R. M. Harrison (2012), Particles, air quality, policy and health, *Chem. Soc. Rev.*, *41*(19), 6606–6630, doi:10.1039/C2CS35076A.

Hoffman, R. C., A. Laskin, and B. J. Finlayson-Pitts (2004), Sodium nitrate particles: Physical and chemical properties during hydration and dehydration, and implications for aged sea salt aerosols, *J. Aerosol Sci.*, *35*(7), 869–887, doi:10.1016/j.jaerosci.2004.02.003.

Hu, M., Z. Wu, J. Slanina, P. Lin, S. Liu, and L. Zeng (2008), Acidic gases, ammonia and water-soluble ions in $PM_{2.5}$ at a coastal site in the Pearl River Delta, China, *Atmos. Environ.*, *42*(25), 6310–6320, doi:10.1016/j.atmosenv.2008.02.015.

Jimenez, J. L., et al. (2009), Evolution of organic aerosols in the atmosphere, *Science*, *326*(5959), 1525–1529, doi:10.1126/science.1180353.

Johnson, E. R., J. Sciegienka, S. Carlos-Cuellar, and V. H. Grassian (2005), Heterogeneous uptake of gaseous nitric acid on dolomite ($CaMg(CO_3)_2$) and calcite ($CaCO_3$) particles: A Knudsen cell study using multiple, single, and fractional particle layers, *J. Phys. Chem. A*, *109*(31), 6901–6911, doi:10.1021/jp0516285.

Kanakidou, M., et al. (2005), Organic aerosol and global climate modelling: A review, *Atmos. Chem. Phys.*, *5*(4), 1053–1123, doi:10.5194/acp-5-1053-2005.

Kawamura, K., and I. R. Kaplan (1987), Motor exhaust emissions as a primary source for dicarboxylic acids in Los Angeles ambient air, *Environ. Sci. Technol.*, *21*(1), 105–110, doi:10.1021/es00155a014.

Kerminen, V. M., K. Teinila, R. Hillamo, and T. Pakkanen (1998), Substitution of chloride in sea-salt particles by inorganic and organic anions, *J. Aerosol Sci.*, *29*(8), 929–942.

Knopf, D. A., B. Wang, A. Laskin, R. C. Moffet, and M. K. Gilles (2010), Heterogeneous nucleation of ice on anthropogenic organic particles collected in Mexico City, *Geophys. Res. Lett.*, *37*, L11803, doi:10.1029/2010GL043362.

Koop, T., J. Bookhold, M. Shiraiwa, and U. Poschl (2011), Glass transition and phase state of organic compounds: Dependency on molecular properties and implications for secondary organic aerosols in the atmosphere, *Phys. Chem. Chem. Phys.*, *13*(43), 19,238–19,255, doi:10.1039/c1cp22617g.

Kroll, J. H., et al. (2011), Carbon oxidation state as a metric for describing the chemistry of atmospheric organic aerosol, *Nat. Chem.*, *3*(2), 133–139.

Krueger, B. J., V. H. Grassian, A. Laskin, and J. P. Cowin (2003), The transformation of solid atmospheric particles into liquid droplets through heterogeneous chemistry: Laboratory insights into the processing of calcium containing mineral dust aerosol in the troposphere, *Geophys. Res. Lett.*, *30*(3), 1148, doi:10.1029/2002GL016563.

Larkin, P. (2011), *IR and Raman Spectroscopy: Principle and Spectral Interpretation*, 228 pp., Elsevier, Mass.

Laskin, A. (2010), Electron beam analysis and microscopy of individual particles, in *Fundamentals and Applications in Aerosol Spectroscopy*, edited by R. Signorell and J. Reid, pp. 463–491, Taylor and Francis, Fla.

Laskin, A., and J. P. Cowin (2001), Automated single-particle SEM/EDX analysis of submicrometer particles down to 0.1 μm, *Anal. Chem.*, *73*(5), 1023–1029, doi:10.1021/ac0009604.

Laskin, A., M. J. Iedema, A. Ichkovich, E. R. Graber, I. Taraniuk, and Y. Rudich (2005a), Direct observation of completely processed calcium carbonate dust particles, *Faraday Discuss.*, *130*, 453–468, doi:10.1039/b417366j.

Laskin, A., T. W. Wietsma, B. J. Krueger, and V. H. Grassian (2005b), Heterogeneous chemistry of individual mineral dust particles with nitric acid: A combined CCSEM/EDX, ESEM, and ICP-MS study, *J. Geophys. Res.*, *110*, D10208, doi:10.1029/2004JD005206.

Laskin, A., J. P. Cowin, and M. J. Iedema (2006), Analysis of individual environmental particles using modern methods of electron microscopy and X-ray microanalysis, *J. Electron Spectrosc. Relat. Phenom.*, *150*(2-3), 260–274.

Laskin, A., R. C. Moffet, M. K. Gilles, J. D. Fast, R. A. Zaveri, B. B. Wang, P. Nigge, and J. Shutthanandan (2012), Tropospheric chemistry of internally mixed sea salt and organic particles: Surprising reactivity of NaCl with weak organic acids, *J. Geophys. Res.*, *117*, D15302, doi:10.1029/2012JD017743.

Laskina, O., M. A. Young, P. D. Kleiber, and V. H. Grassian (2013), Infrared extinction spectroscopy and micro-Raman spectroscopy of select components of mineral dust mixed with organic compounds, *J. Geophys. Res. Atmos.*, *118*, 6593–6606, doi:10.1002/jgrd.50494.

Lefer, B. L., R. W. Talbot, and J. W. Munger (1999), Nitric acid and ammonia at a rural northeastern U.S. site, *J. Geophys. Res.*, *104*(D1), 1645–1661, doi:10.1029/1998JD100016.

Lewis, E. R., and S. E. Schwartz (2004), *Sea Salt Aerosol Production: Mechanisms, Methods, Measurements and Models—A Critical Review*, 412 pp., AGU, Washington, D. C.

Li, X., et al. (2012), Exploring the atmospheric chemistry of nitrous acid (HONO) at a rural site in southern China, *Atmos. Chem. Phys.*, *12*(3), 1497–1513, doi:10.5194/acp-12-1497-2012.

Liu, Y., J. P. Cain, H. Wang, and A. Laskin (2007), Kinetic study of heterogeneous reaction of deliquesced NaCl particles with gaseous HNO_3 using particle-on-substrate stagnation flow reactor approach, *J. Phys. Chem. A*, *111*(40), 10,026–10,043, doi:10.1021/jp072005p.

Liu, Y., Z. Yang, Y. Desyaterik, P. L. Gassman, H. Wang, and A. Laskin (2008), Hygroscopic behavior of substrate-deposited particles studied by micro-FT-IR spectroscopy and complementary methods of particle analysis, *Anal. Chem.*, *80*(3), 633–642, doi:10.1021/ac701638r.

Liu, Y., et al. (2011), Internal structure, hygroscopic and reactive properties of mixed sodium methanesulfonate-sodium chloride particles, *Phys. Chem. Chem. Phys.*, *13*(25), 11,846–11,857, doi:10.1039/C1CP20444K.

Lohmann, U., and J. Feichter (2005), Global indirect aerosol effects: A review, *Atmos. Chem. Phys.*, *5*(3), 715–737, doi:10.5194/acp-5-715-2005.

Loukhovitskaya, E. E., R. K. Talukdar, and A. R. Ravishankara (2013), Uptake of HNO_3 on aviation kerosene and aircraft engine soot: Influences of H_2O or/and H_2SO_4, *J. Phys. Chem. A*, *117*(23), 4928–4936, doi:10.1021/jp401723k.

Ma, Q., Y. Liu, C. Liu, and H. He (2012), Heterogeneous reaction of acetic acid on MgO, a-Al_2O_3, and $CaCO_3$ and the effect on the hygroscopic behaviour of these particles, *Phys. Chem. Chem. Phys.*, *14*(23), 8403–8409, doi:10.1039/C2CP40510E.

Ma, Q., J. Ma, C. Liu, C. Lai, and H. He (2013), Laboratory study on the hygroscopic behavior of external and internal C2–C4 dicarboxylic acid–NaCl mixtures, *Environ. Sci. Technol.*, *47*(18), 10,381–10,388, doi:10.1021/es4023267.

Mahowald, N. M., A. R. Baker, G. Bergametti, N. Brooks, R. A. Duce, T. D. Jickells, N. Kubilay, J. M. Prospero, and I. Tegen (2005), Atmospheric global dust cycle and iron inputs to the ocean, *Global Biogeochem. Cycles*, *19*, GB4025, doi:10.1029/2004GB002402.

Mikhailov, E., S. Vlasenko, S. T. Martin, T. Koop, and U. Poschl (2009), Amorphous and crystalline aerosol particles interacting with water vapor: Conceptual framework and experimental evidence for restructuring, phase transitions and kinetic limitations, *Atmos. Chem. Phys.*, *9*(24), 9491–9522.

Moffet, R. C., et al. (2008), Characterization of aerosols containing Zn, Pb, and Cl from an industrial region of Mexico City, *Environ. Sci. Technol.*, *42*(19), 7091–7097, doi:10.1021/es7030483.

Moffet, R. C., et al. (2010), Microscopic characterization of carbonaceous aerosol particle aging in the outflow from Mexico City, *Atmos. Chem. Phys.*, *10*(3), 961–976, doi:10.5194/acp-10-961-2010.

Morino, Y., Y. Kondo, N. Takegawa, Y. Miyazaki, K. Kita, Y. Komazaki, M. Fukuda, T. Miyakawa, N. Moteki, and D. R. Worsnop (2006), Partitioning of HNO_3 and particulate nitrate over Tokyo: Effect of vertical mixing, *J. Geophys. Res.*, *111*, D15215, doi:10.1029/2005JD006887.

Moussa, S. G., A. C. Stern, J. D. Raff, C. W. Dilbeck, D. J. Tobias, and B. J. Finlayson-Pitts (2013), Experimental and theoretical studies of the interaction of gas phase nitric acid and water with a self-assembled monolayer, *Phys. Chem. Chem. Phys.*, *15*(2), 448–458, doi:10.1039/C2CP42405C.

Murphy, D. M., D. J. Cziczo, K. D. Froyd, P. K. Hudson, B. M. Matthew, A. M. Middlebrook, R. E. Peltier, A. Sullivan, D. S. Thomson, and R. J. Weber (2006), Single-particle mass spectrometry of tropospheric aerosol particles, *J. Geophys. Res.*, *111*, D23S32, doi:10.1029/2006JD007340.

Peng, C., and C. K. Chan (2001), The water cycles of water-soluble organic salts of atmospheric importance, *Atmos. Environ.*, *35*(7), 1183–1192, doi:10.1016/s1352-2310(00)00426-x.

Peng, C., M. N. Chan, and C. K. Chan (2001), The hygroscopic properties of dicarboxylic and multifunctional acids: Measurements and UNIFAC predictions, *Environ. Sci. Technol.*, *35*(22), 4495–4501, doi:10.1021/es0107531.

Pöschl, U. (2005), Atmospheric aerosols: Composition, transformation, climate and health effects, *Angew. Chem., Int. Ed.*, *44*(46), 7520–7540, doi:10.1002/anie.200501122.

Qiu, C., and R. Zhang (2013), Multiphase chemistry of atmospheric amines, *Phys. Chem. Chem. Phys.*, *15*(16), 5738–5752, doi:10.1039/C3CP43446J.

Ramanathan, V., P. J. Crutzen, J. T. Kiehl, and D. Rosenfeld (2001), Aerosols, climate, and the hydrological cycle, *Science*, *294*(5549), 2119–2124, doi:10.1126/science.1064034.

Ravishankara, A. R. (1997), Heterogeneous and multiphase chemistry in the troposphere, *Science*, *276*(5315), 1058–1065, doi:10.1126/science.276.5315.1058.

Rehbein, P. J. G., C.-H. Jeong, M. L. McGuire, X. Yao, J. C. Corbin, and G. J. Evans (2011), Cloud and fog processing enhanced gas-to-particle partitioning of trimethylamine, *Environ. Sci. Technol.*, *45*(10), 4346–4352, doi:10.1021/es1042113.

Ribeiro da Silva, M. A. V., M. J. S. Monte, and J. R. Ribeiro (1999), Vapour pressures and the enthalpies and entropies of sublimation of five dicarboxylic acids, *J. Chem. Thermodyn.*, *31*(8), 1093–1107.

Ro, C. U., J. Osan, and R. van Grieken (1999), Determination of low-Z elements in individual environmental particles using windowless EPMA, *Anal. Chem.*, *71*(8), 1521–1528, doi:10.1021/ac981070f.

Ro, C. U., J. Osan, I. Szaloki, K. Y. Oh, H. Kim, and R. Van Grieken (2000), Determination of chemical species in individual aerosol particles using ultrathin window EPMA, *Environ. Sci. Technol.*, *34*(14), 3023–3030, doi:10.1021/es9910661.

Ro, C. U., K. Y. Oh, J. Osan, J. de Hoog, A. Worobiec, and R. Van Grieken (2001), Heterogeneity assessment in individual $CaCO_3$-$CaSO_4$ particles using ultrathin window electron probe X-ray microanalysis, *Anal. Chem.*, *73*(19), 4574–4583, doi:10.1021/ac010438x.

Rosenfeld, D. (2000), Suppression of rain and snow by urban and industrial air pollution, *Science*, *287*, (5459), 1793–1796, doi:10.1126/science.287.5459.1793.

Rossi, M. J. (2003), Heterogeneous reactions on salts, *Chem. Rev.*, *103*(12), 4823–4882, doi:10.1021/cr020507n.

Rubasinghege, G., and V. H. Grassian (2013), Role(s) of adsorbed water in the surface chemistry of environmental interfaces, *Chem. Commun.*, *49*(30), 3071–3094, doi:10.1039/C3CC38872G.

Rudich, Y. (2003), Laboratory perspectives on the chemical transformations of organic matter in atmospheric particles, *Chem. Rev.*, *103*(12), 5097–5124, doi:10.1021/cr020508f.

Salgado Munoz, M. S., and M. J. Rossi (2002), Heterogeneous reactions of HNO_3 with flame soot generated under different combustion conditions. Reaction mechanism and kinetics, *Phys. Chem. Chem. Phys.*, *4*(20), 5110–5118, doi:10.1039/B203912P.

Salo, K., Å. M. Jonsson, P. U. Andersson, and M. Hallquist (2010), Aerosol volatility and enthalpy of sublimation of carboxylic acids, *J. Phys. Chem. A*, *114*(13), 4586–4594, doi:10.1021/jp910105h.

Saxena, P., and L. Hildemann (1996), Water-soluble organics in atmospheric particles: A critical review of the literature and application of thermodynamics to identify candidate compounds, *J. Atmos. Chem.*, *24*(1), 57–109, doi:10.1007/BF00053823.

Seidell, A. (1919), *Solubilities of Inorganic and Organic Compounds*, 2nd ed., D. Van Nostrand Company, New York.

Seinfeld, J., and S. Pandis (1998), *Atmospheric Chemistry and Physics: From Air Pollution to Climate Change*, John Wiley, New York.

Shiraiwa, M., M. Ammann, T. Koop, and U. Pöschl (2011), Gas uptake and chemical aging of semisolid organic aerosol particles, *Proc. Natl. Acad. Sci. U. S. A.*, *108*(27), 11,003–11,008, doi:10.1073/pnas.1103045108.

Song, Y. C., H. J. Eom, H. J. Jung, M. A. Malek, H. K. Kim, H. Geng, and C. U. Ro (2013), Investigation of aged Asian dust particles by the combined use of quantitative ED-EPMA and ATR-FTIR imaging, *Atmos. Chem. Phys.*, *13*(6), 3463–3480, doi:10.5194/acp-13-3463-2013.

Soonsin, V., A. A. Zardini, C. Marcolli, A. Zuend, and U. K. Krieger (2010), The vapor pressures and activities of dicarboxylic acids reconsidered: The impact of the physical state of the aerosol, *Atmos. Chem. Phys.*, *10*(23), 11,753–11,767, doi:10.5194/acp-10-11753-2010.

Stone, E. A., C. J. Hedman, J. Zhou, M. Mieritz, and J. J. Schauer (2010), Insights into the nature of secondary organic aerosol in Mexico City during the MILAGRO experiment 2006, *Atmos. Environ.*, *44*(3), 312–319.

Tong, S. R., L. Y. Wu, M. F. Ge, W. G. Wang, and Z. F. Pu (2010), Heterogeneous chemistry of monocarboxylic acids on a-Al_2O_3 at different relative humidities, *Atmos. Chem. Phys.*, *10*(16), 7561–7574, doi:10.5194/acp-10-7561-2010.

Usher, C. R., A. E. Michel, and V. H. Grassian (2003), Reactions on mineral dust, *Chem. Rev.*, *103*(12), 4883–4939.

Vlasenko, A., T. Huthwelker, H. W. Gaggeler, and M. Ammann (2009), Kinetics of the heterogeneous reaction of nitric acid with mineral dust particles: An aerosol flowtube study, *Phys. Chem. Chem. Phys.*, *11*(36), 7921–7930, doi:10.1039/B904290N.

Wang, B., A. T. Lambe, P. Massoli, T. B. Onasch, P. Davidovits, D. R. Worsnop, and D. A. Knopf (2012a), The deposition ice nucleation and immersion freezing potential of amorphous secondary organic aerosol: Pathways for ice and mixed-phase cloud formation, *J. Geophys. Res.*, *117*, D16209, doi:10.1029/2012JD018063.

Wang, B., A. Laskin, T. Roedel, M. K. Gilles, R. C. Moffet, A. V. Tivanski, and D. A. Knopf (2012b), Heterogeneous ice nucleation and water uptake by field-collected atmospheric particles below 273 K, *J. Geophys. Res.*, *117*, D00V19, doi:10.1029/2012JD017446.

Wijenayaka, L. A., G. Rubasinghege, J. Baltrusaitis, and V. H. Grassian (2012), Surface chemistry of α-FeOOH nanorods and microrods with gas-phase nitric acid and water vapor: Insights into the role of particle size, surface structure, and surface hydroxyl groups in the adsorption and reactivity of α-FeOOH with atmospheric gases, *J. Phys. Chem. A*, *116*(23), 12,566–12,577, doi:10.1021/jp301139x.

Wise, M. E., J. D. Surratt, D. B. Curtis, J. E. Shilling, and M. A. Tolbert (2003), Hygroscopic growth of ammonium sulfate/dicarboxylic acids, *J. Geophys. Res.*, *108*(D20), 4638 doi:10.1029/2003JD003775.

Wu, Z. J., A. Nowak, L. Poulain, H. Herrmann, and A. Wiedensohler (2011), Hygroscopic behavior of atmospherically relevant water-soluble carboxylic salts and their influence on the water uptake of ammonium sulfate, *Atmos. Chem. Phys.*, *11*(24), 12,617–12,626, doi:10.5194/acp-11-12617-2011.

Yang, L., and L. E. Yu (2008), Measurements of oxalic acid, oxalates, malonic acid, and malonates in atmospheric particulates, *Environ. Sci. Technol.*, *42*(24), 9268–9275, doi:10.1021/es801820z.

You, Y., et al. (2012), Images reveal that atmospheric particles can undergo liquid–liquid phase separations, *Proc. Natl. Acad. Sci. U. S. A.*, *109*(33), 13,188–13,193, doi:10.1073/pnas.1206414109.

Zhang, Q., et al. (2007), Ubiquity and dominance of oxygenated species in organic aerosols in anthropogenically-influenced Northern Hemisphere midlatitudes, *Geophys. Res. Lett.*, *34*, L13801, doi:10.1029/2007GL029979.

Zhang, G.,X. Bi, L. Y. Chan, L. Li, X. Wang, J. Feng, G. Sheng, J. Fu, M. Li, and Z. Zhou (2012), Enhanced trimethylamine-containing particles during fog events detected by single particle aerosol mass spectrometry in urban Guangzhou, China, *Atmos. Environ.*, *55*(0), 121–126, doi:10.1016/j.atmosenv.2012.03.038.

Zheng, J., et al. (2008), Measurements of HNO_3 and N_2O_5 using ion drift-chemical ionization mass spectrometry during the MILAGRO/MCMA-2006 campaign, *Atmos. Chem. Phys.*, *8*(22), 6823–6838, doi:10.5194/acp-8-6823-2008.

Ziemba, L. D., J. E. Dibb, R. J. Griffin, C. H. Anderson, S. I. Whitlow, B. L. Lefer, B. Rappenglück, and J. Flynn (2010), Heterogeneous conversion of nitric acid to nitrous acid on the surface of primary organic aerosol in an urban atmosphere, *Atmos. Environ.*, *44*(33), 4081–4089.